CHAPTER 5

Synthesis of Ni-Zn Ferrite nanopowders by using PVA precursor based method

5.1 Experimental Procedure for Chemical Synthesis:

The chemicals used were $Fe(NO_3)_3.9H_2O$ (99.9%, Merck, India), $Ni(NO_3)_2.6H_2O$ (99.9%, Merck, India), Zn dust (99.9%, Merck, India), PVA (polyvinyl alcohol) of mol. wt. 1,25,000 (99.9%, Merck, India) and sucrose (99.9%, Merck, India) without further purification. $Zn(NO_3)_2$ was prepared by dissolving Zn powder in aqueous nitric acid.

Stoichiometric amounts of metal nitrates were dissolved in distilled water according to the molar compositions as shown in Table 5.1.

Table 5.1. Molar ratio of starting compounds.

Target Composition	$Fe(NO_3)_3.9H_2O$	$Ni(NO_3)_2.6H_2O$	Zn powder	PVA monomer unit	Sucrose
$Ni_{0.80}Zn_{0.20}Fe_2O_4$	0.084	0.034	0.008	0.315	0.0315
$Ni_{0.65}Zn_{0.35}Fe_2O_4$	0.084	0.027	0.015	0.315	0.0315
$Ni_{0.50}Zn_{0.50}Fe_2O_4$	0.084	0.021	0.021	0.315	0.0315
$Ni_{0.40}Zn_{0.60}Fe_2O_4$	0.084	0.017	0.025	0.315	0.0315

Aqueous solutions of metal nitrates and PVA were mixed in a molar ratio of 1:2.5. An aqueous solution of sucrose (10 wt% of sucrose with respect to PVA) was added to this mixture and stirred for 1hour at room temperature.The solutions were stirred for 1hour at room temperature using a magnetic stirrer.

Dark brown precursors were formed when the mixtures were evaporated to dryness on a hot plate at ~125^{0}C. The precursor powders were then calcined in air in temperatures ranging from 650 to 950^{0}C for two and a half hours in air to obtain Ni-Zn ferrite nanopowders [133]. In order to avoid contamination of the precursors by carbon, a few drops of saturated ammonium nitrate solution was added to the precursor powders during calcination.

5.2 Results and Discussion:

5.2.1 Thermal Analysis:

TG-DTG and DSC analyses were performed to investigate the decomposition behavior of the precursor powders due to heat treatment in air and thermograms are shown in Fig 5.1(a-d).

The important features of the thermograms are as follows:

(i) In TG thermogram, a total weight loss of ~ 75% in all precursors (x = 0.20, 0.35, 0.50 and 0.60) was observed when the sample was heated between 40 to 950^{0}C in air.

(ii) Weight loss of ~20% occurred between 40 and 200^{0}C that can be assigned to the loss of moisture from the samples followed by strongly adsorbed water molecules.

(iii) Major weight loss of ~55% occurred in the region from 200 to 550^{0}C and this weight loss was attributed to the oxidative decomposition of the organic components of the precursor leading to the evolution of NO_x and CO_2 gases.

(iv) The oxidative decomposition was reflected in DSC thermogram as exothermic peaks at 332, 334, 337 and 346^{0}C for x = 0.20, 0.35, 0.50 and 0.60 respectively.

(v) Heating the sample beyond 550^{0}C did not result in a significant weight loss in the samples. The trivial weight loss (~1-2%) beyond this temperature was only due to slow oxidation of carbonaceous material in the precursor.

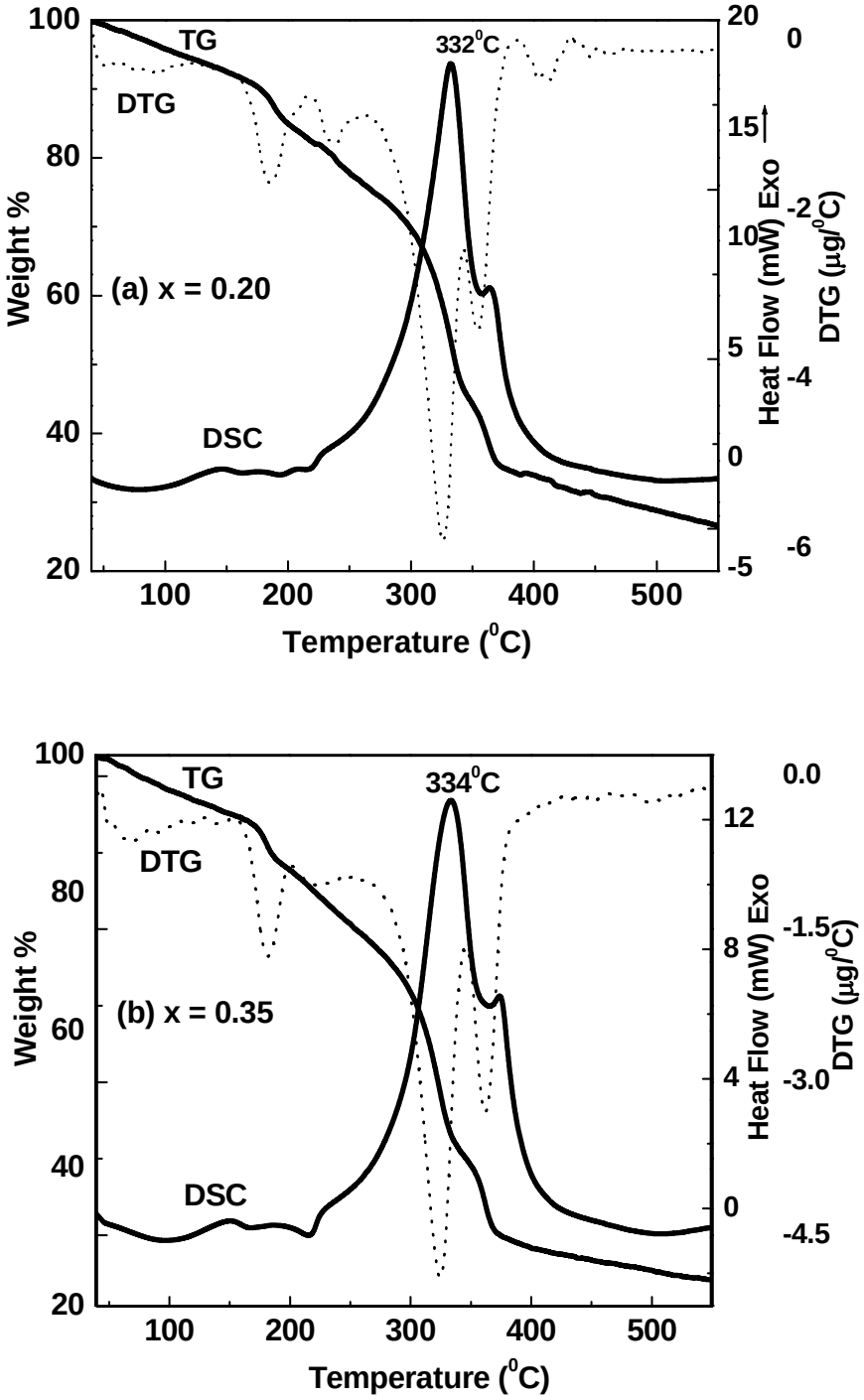

Fig 5.1 continued

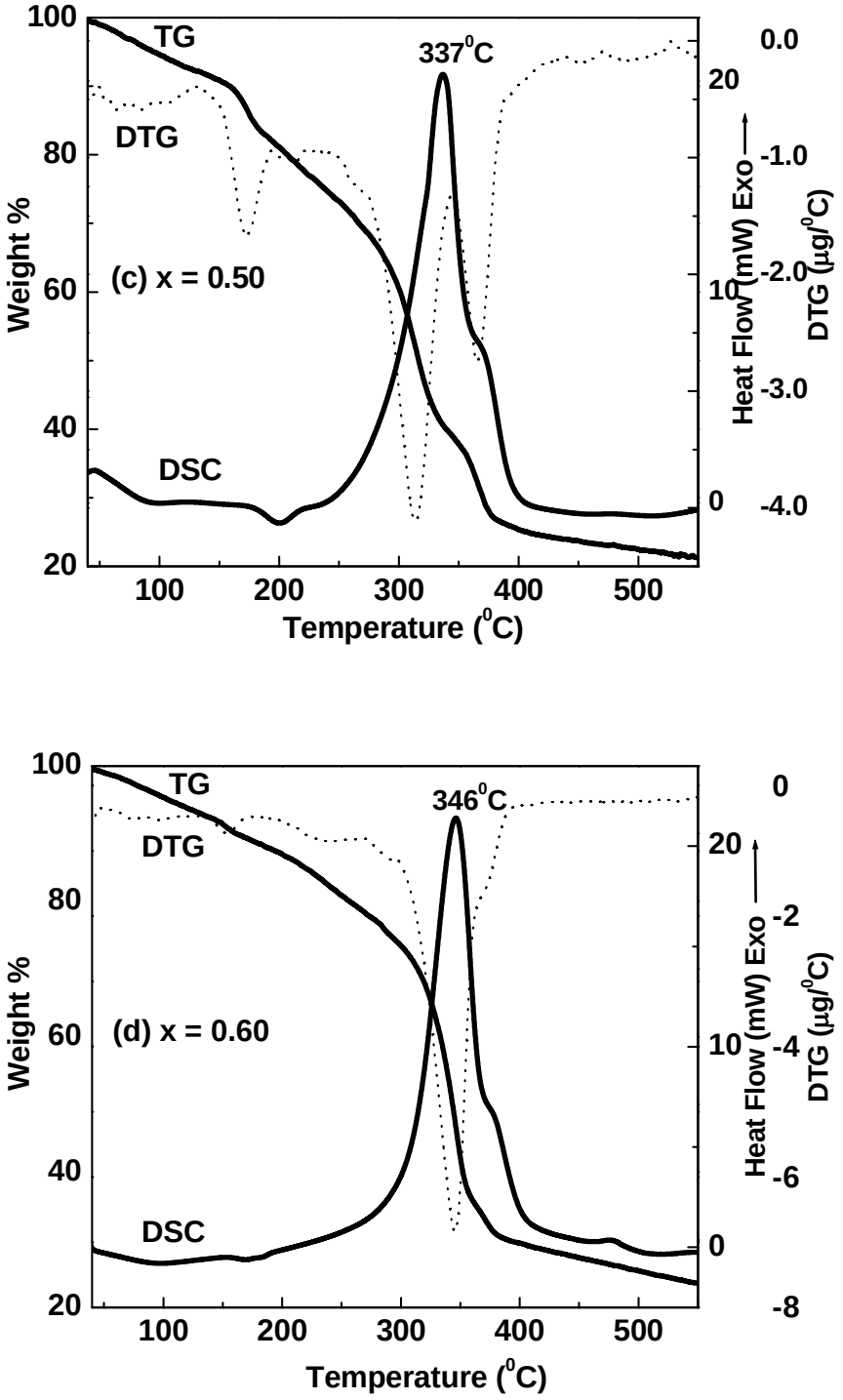

Fig. 5.1 TG-DTG and DSC thermograms of precursor powders of (a) $Ni_{0.80}Zn_{0.20}Fe_2O_4$ (b) $Ni_{0.65}Zn_{0.35}Fe_2O_4$ (c) $Ni_{0.50}Zn_{0.50}Fe_2O_4$ and (d) $Ni_{0.40}Zn_{0.60}Fe_2O_4$ in air.

The DSC thermograms of the series of precursors were compared and are shown in Fig. 5.2. The exothermic peak corresponding to the oxidative decomposition shifted from 346 to 332^{0}C with increase in Ni^{2+} concentration from (1-x) = 0.40 to 0.80 in the $Ni_{1-x}Zn_xFe_2O_4$ composition. This decrease in decomposition temperature with increase in Ni^{2+} concentration was due to the catalyzing effect of Ni^{2+} on the decomposition process. The heat liberated (4 - 5 kJ/g, depending upon the composition) through this process was sufficient for the crystallization of the desired ferrite phase [133, 134].

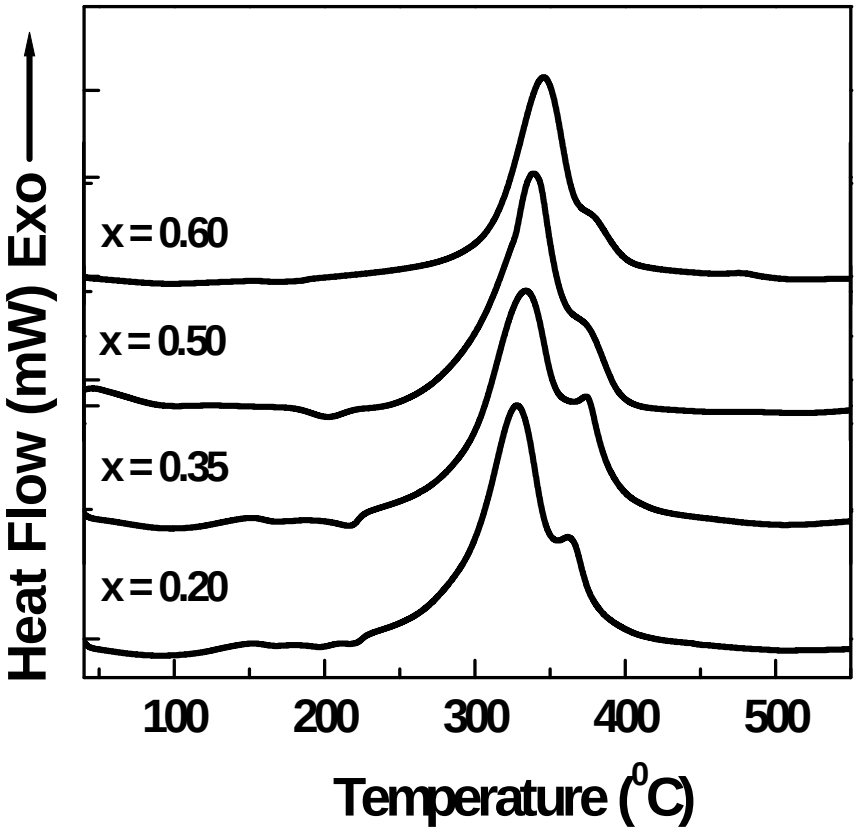

Fig 5.2 DSC thermograms of precursors powders for the series of $Ni_{1-x}Zn_xFe_2O_4$ ferrites.

5.2.2 XRD Analysis:

Room temperature XRD spectra of powders, calcined at different temperatures for all values of x are shown in Fig. 5.3 (a-d).

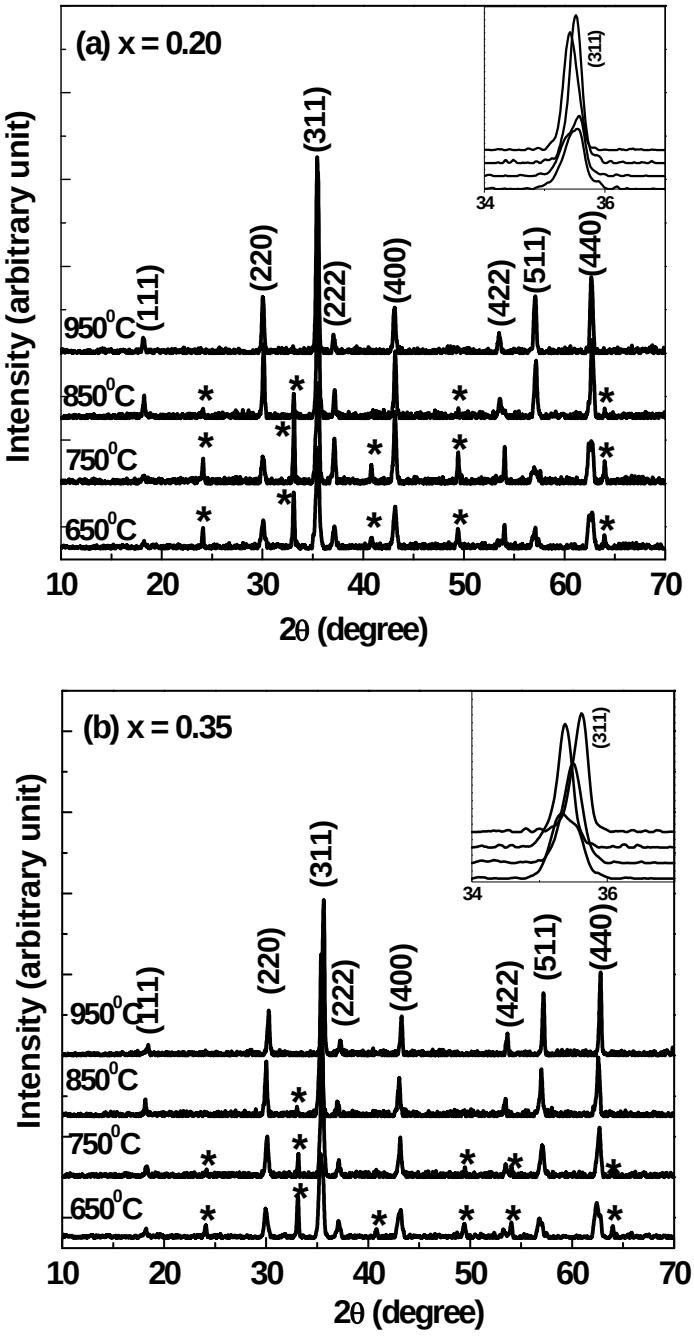

Fig. 5.3 continued

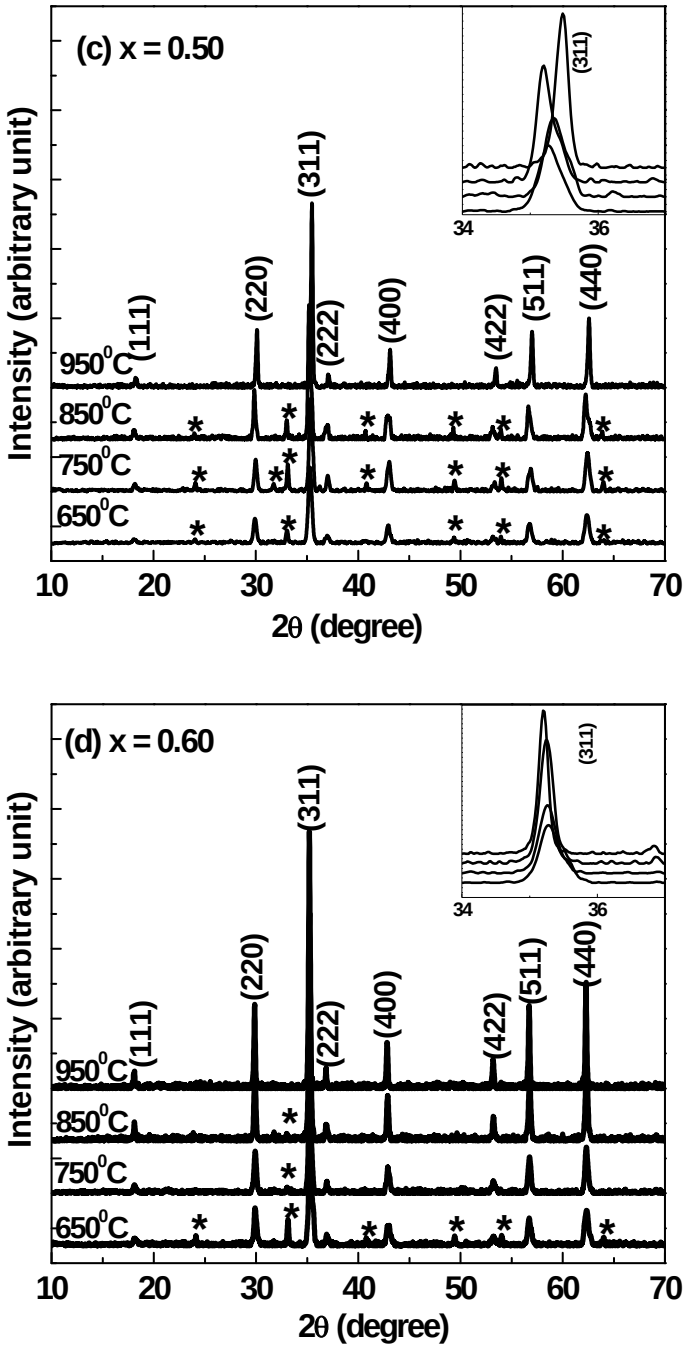

Fig. 5.3 XRD spectra of precursor powders of (a) $Ni_{0.80}Zn_{0.20}Fe_2O_4$ (b) $Ni_{0.65}Zn_{0.35}Fe_2O_4$ (c) $Ni_{0.50}Zn_{0.50}Fe_2O_4$ (d) $Ni_{0.40}Zn_{0.60}Fe_2O_4$ ferrites, at different calcination temperatures. Slow scan of the (311) diffraction plane are shown in the insets. Impurity phase is marked by (*) and corresponds to pure hematite.

The main features of the spectra are as follows:

(i) The appearance of the main intensity peaks corresponding to (311) diffraction planes for powder calcined at 650^0C, indicated the beginning of the formation of Ni-Zn ferrite phase.

(ii) Although Ni-Zn ferrite phase was present for each precursor powder calcined at different temperatures, peaks corresponding to α-Fe_2O_3 (hematite) as an impurity phase were also present. The peaks for impurity phase are marked as (*) and correspond to (012), (104), (113), (024) and (300) diffraction planes of pure hematite (JCPDS 80-2377).

(iii) Complete formation of single-phase Ni-Zn ferrite occurred when precursor was calcined at 950^0C for two and a half hours in air [133]. Peaks corresponding to (111), (220), (311), (222), (400), (422), (511) and (440) diffraction planes of Ni-Zn ferrite were present for the pure phase (JCPDS 08-0234).

(iv) Crystallite size of powders calcined at different temperatures was calculated using Scherrer's equation [125] and they lie in the range of 20-50 nm depending upon the calcination temperature.

5.2.3 TEM Analysis:

The TEM micrographs for the powders calcined at 950^0C are shown in Fig. 5.4 (a) and (b). The micrographs clearly indicated that average particle size of the calcined powder was ~50 nm and it matched well with that calculated from XRD data. The particles were mostly round in shape and formed loose aggregates.

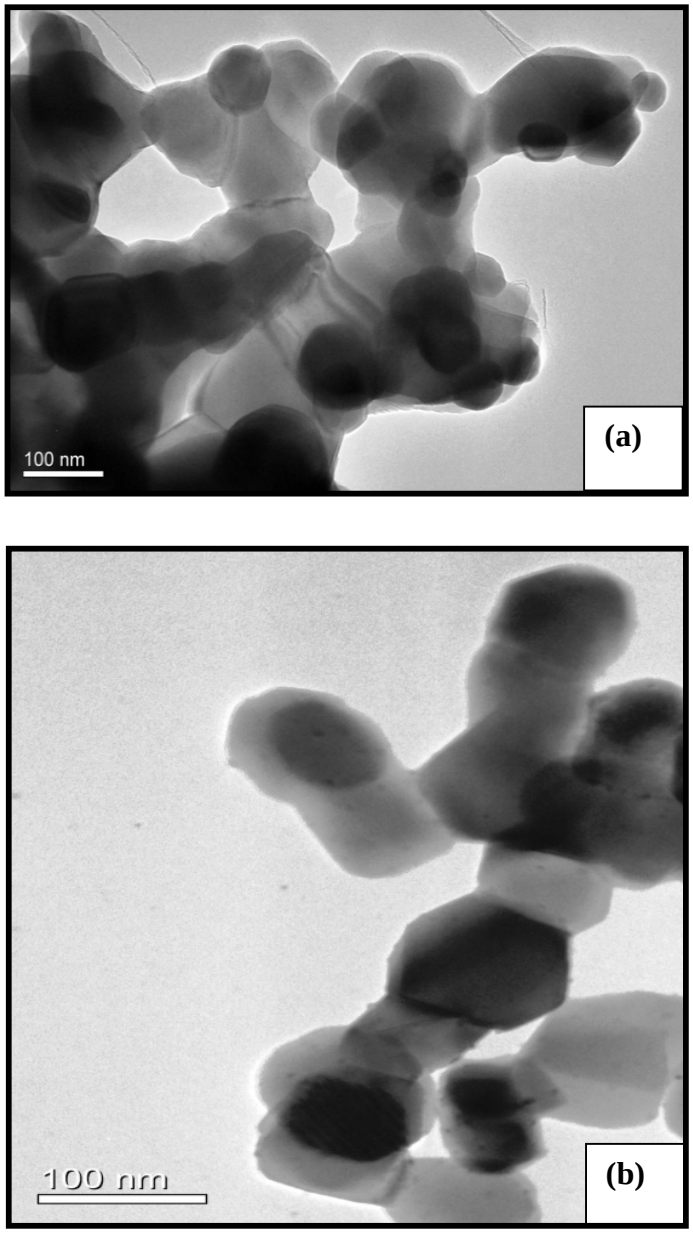

Fig 5.4 TEM micrographs for the series of $Ni_{1-x}Zn_xFe_2O_4$ of nanopowders for (a) x = 0.35 and (b) x = 0.50, synthesized at a calcination temperature of 950^0C.

5.2.4 SEM Analysis:

SEM was used to investigate the change of microstructures of the as synthesized $Ni_{1-x}Zn_xFe_2O_4$ nanopowders with change in sintering temperature and composition and these are shown in Fig 5.5 (a-i).

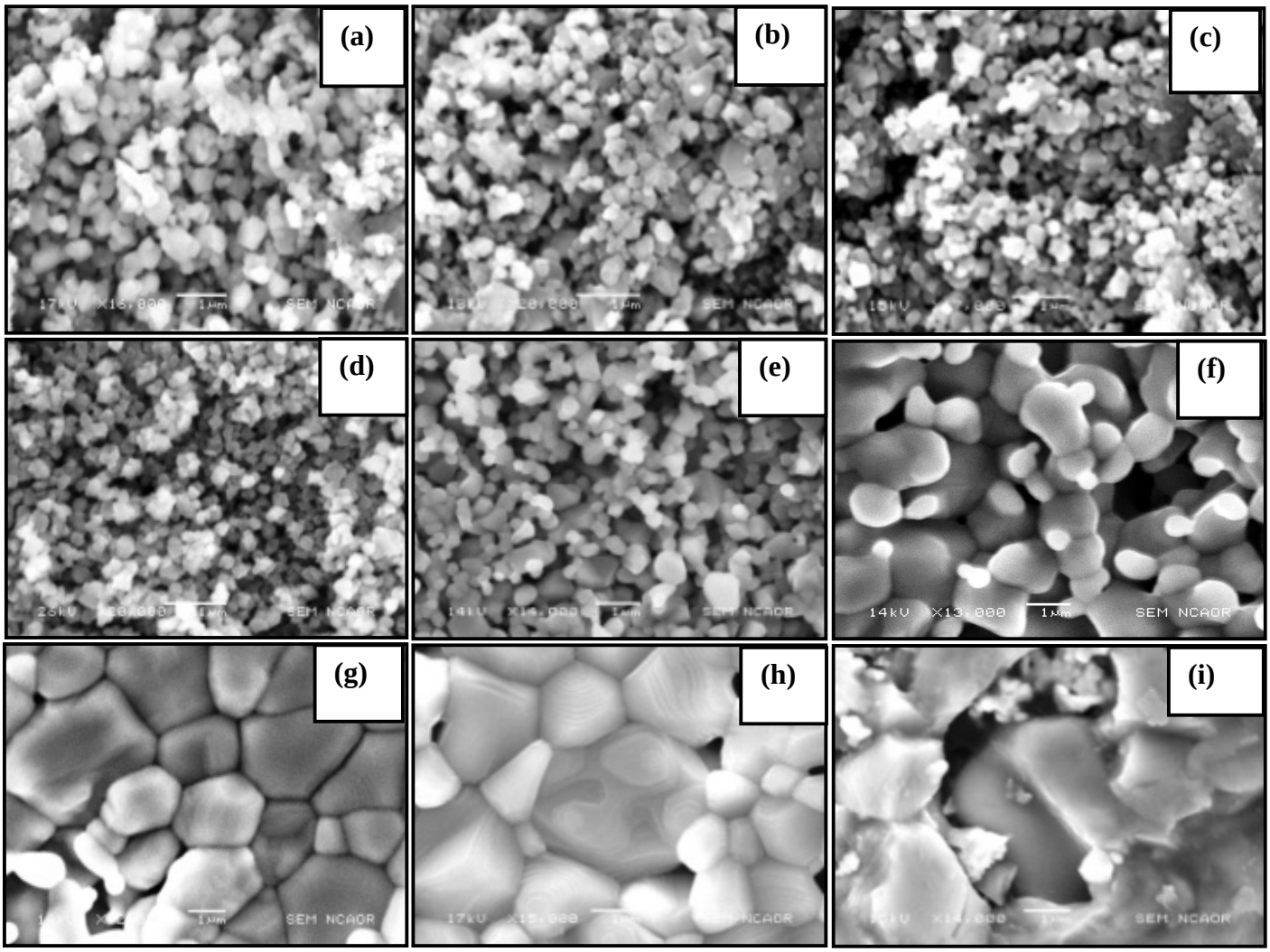

Fig. 5.5.SEM micrographs of $Ni_{1-x}Zn_xFe_2O_4$ showing the change of microstructure with changing value of x and sintering condition (a) x= 0.2, unsintered, (b) x= 0.35, unsintered, (c) x= 0.5, unsintered, (d) x= 0.6, unsintered, (e) x= 0.2, sintered at 1100^0C, (f) x= 0.2, sintered at 1200^0C, (g) x= 0.2, sintered at 1200^0C, (h) x= 0.2, sintered at 1300^0C and (i) x= 0.6, sintered at 1300^0C.

For this purpose, four sets of pellets were prepared; (i) one pellet was kept unsintered (ii) the other set of pellets were sintered at 1100, 1200 and 1300^0C. The SEM results of the as-synthesized nanopowders (unsintered) and sintered samples can be summarized as follows:

(i) SEM micrographs of the unsintered samples revealed uniform, agglomerated and spherical shaped nanopowders of Ni-Zn ferrite (Fig. 5.5(a-d)).

(ii) When sintering temperature was 1100^0C, the grains grew to micron size and agglomeration was present. The samples also exhibited high intergranular porosity (Fig. 5.5(e)).

(iii) Sintering at 1200^0C resulted in formation of well-defined bigger grain sizes but average grain size was still less than 3 μm (Fig. 5.5(f-g)). Though sintering temperature was reasonably high (1200^0C), Zn loss was not observed in our samples which ensures the maintenance of stoichiometry of the final product. Inhomogeneity or partial precipitation of impurity phase was not observed for our samples whereas in most of the reported results, Zn loss at high temperatures has been observed in SEM micrographs as pore formation within the grains [66-68].

(iv) When sintering was performed at 1300^0C, formation of bigger grains occurred but their grain size distribution became non-uniform, particularly when concentration of Zn is high. In case of x = 0.20, grains with clear boundary were observed, but when x = 0.60, well-defined microstructure was destroyed (Fig. 5.5(h-i)).

5.2.5 DC Resistivity measurement:

DC resistivity of the unsintered and sintered pellets at 1100 and 1200^0C was measured from room temperature (25^0C) to 225^0C for all values of x and its variation with temperature is shown in Fig. 5.6.Room temperature resistivity values for the series of composition ($Ni_{1-x}Zn_xFe_2O_4$ with x = 0.20, 0.35, 0.50 and 0.60) sintered at various temperatures are listed in Table 5.2.

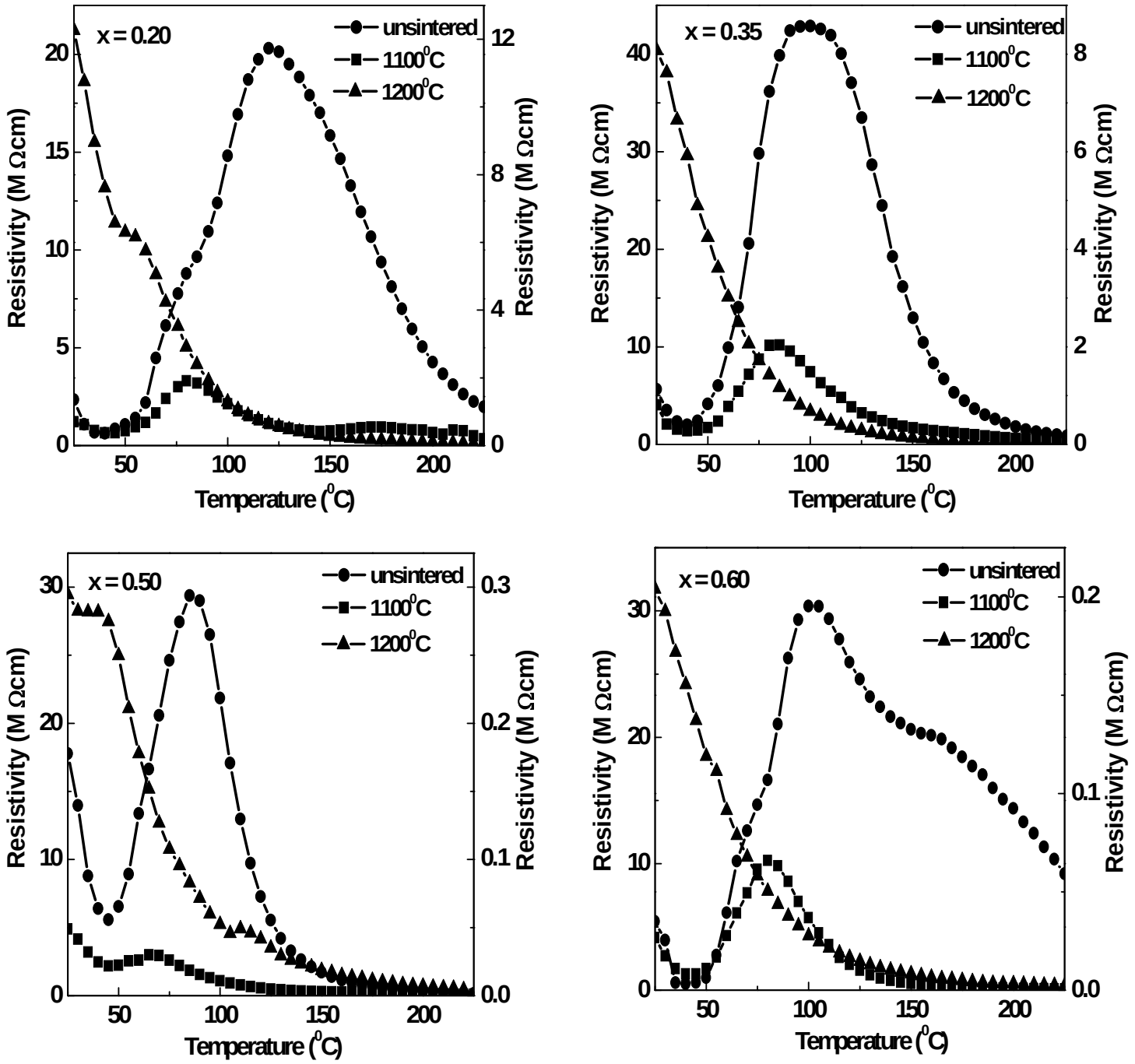

Fig 5.6 DC resistivity for the series of $Ni_{1-x}Zn_xFe_2O_4$ (x = 0.20, 0.35, 0.50 and 0.60) nanopowders with respect to temperature for unsintered samples and samples sintered at 1100 and 1200^{0}C. Left Y axis is the scale for unsintered samples and samples sintered at 1100^{0}C. Right Y axis is the scale for samples sintered at 1200^{0}C.

Table 5.2. Room temperature (25^0C) DC resistivity of Ni-Zn ferrites for unsintered samples and samples sintered at 1100 and 1200^0C.

Composition $Ni_{1-x}Zn_xFe_2O_4$	DC Resistivity (Ω cm)		
	Unsintered	1100^0C	1200^0C
x = 0.20	2.3×10^6	1.2×10^6	1.2×10^7
x = 0.35	5.6×10^6	4.1×10^6	8.1×10^6
x = 0.50	1.8×10^7	4.9×10^6	2.9×10^5
x = 0.60	5.4×10^6	4.1×10^6	2.0×10^5

The impact of microstructure, sintering temperature and composition of the series of $Ni_{1-x}Zn_xFe_2O_4$ ($0 < x < 1$) nanopowders on the resistivity are discussed below.

(i) Impact of microstructure:

It was observed that the room temperature resistivity of the unsintered samples was of the order of ~10^6-10^7Ω cm. With increase in temperature, the resistivity increased and a maximum was recorded in the temperature range of ~ 80-100^0C for all values of x. This behavior might be attributed to the presence of open porosity, loose agglomeration of ultrafine powders and entrapped moisture inside the pores of the powders (humidity recorded in our lab was ~91% at room temperature) [12, 13, 133, 135]. Increasing the temperature up to ~100^0C caused the evaporation of moisture from the samples and therefore, maximum resistivity was attained. This maximum in resistivity corresponds to desorption of moisture from the samples [12, 13, 123,

126, 131, 135]. Beyond ~100^0C, the samples exhibited typical negative temperature coefficient of resistance (NTCR) behavior of ferrites [38]. Such high resistivities can be explained by simply understanding the fact that smaller grains would offer greater resistance to electron path.

When the samples were sintered at 1100^0C, the grains grew in size and also the porosity was reduced. Although the room temperature resistivity values of the samples sintered at 1100^0C are quite similar to unsintered nanopowders but the effect of moisture in these samples was less pronounced due to lesser porosity (as seen in SEM micrographs).This was indicated by the complete loss of moisture at a temperature lower than ~100^0C (Fig.5.6 (a-d)) for all values of x due to fewer number of pores.

The microstructures of samples sintered at 1200^0C revealed the absence of any intergranular porosity especially for higher Zn concentration (x = 0.60). Therefore, these samples exhibited typical NTCR behavior of ferrites from room temperature to 225^0C.

(ii) Impact of sintering temperature:

Increasing the sintering temperature of the samples from 1100 to 1200^0C resulted in moderate increase in room temperature resistivity for the samples with x = 0.20 and 0.35, whereas resistivity decreased for x = 0.50 and 0.60 (Table 5.2). For lower values of x, the increase in resistivity may be attributed to the definite grain size and well defined grain boundaries of the samples as compared to the microstructure of nanopowders (as seen in SEM, Fig 5.5 (a), (b)). For higher values of x, the presence of zinc in the samples dominated over microstructure and resulted in larger grains with lesser number of grain boundaries and hence a decrease in the room temperature resistivity of the samples was observed.

(iii) Impact of Zn content on the series of $Ni_{1-x}Zn_xFe_2O_4$ ($0 < x < 1$) powders:

Room temperature resistivity of the unsintered samples and samples sintered at 1100^0C did not exhibit much dependence on the amount of zinc in the samples (Table 5.2). This is probably due to the particle size of the nanopowders being almost of the same size irrespective of the composition and restricted grain growth of particles even on being sintered at 1100^0C.

Unlike for the unsintered and sintered samples at 1100^0C, the room temperature resistivity of the samples sintered at 1200^0C was dependent on the composition of the samples. A decrease in resistivity from ~10^7 to ~10^5Ωcm was observed when x changes from x = 0.20 to x = 0.60. The reduction in resistivity on increasing the x value can be attributed to increase in the zinc content that resulted in higher amount of densification and bigger grain sizes with lesser number of insulating grain boundaries [66].

5.2.6 Magnetization Measurement:

Room temperature saturation magnetization (M_s) and coercivity (H_c) of the as-synthesized nanopowders was measured and the hysteresis loops for all compositions are shown in Fig. 5.7. The measured values for the series of composition $Ni_{1-x}Zn_xFe_2O_4$ ($0 < x < 1$) are listed in Table 5.3.

Table 5.3 Room temperature saturation magnetization and coercivity of different compositions.

$Ni_{1-x}Zn_xFe_2O_4$	M_s (emu/g)	H_c (Oe)
x = 0.20	61.1	58.4
x = 0.35	59.9	43.5
x = 0.50	51.2	73.1
x = 0.60	49.3	16.3

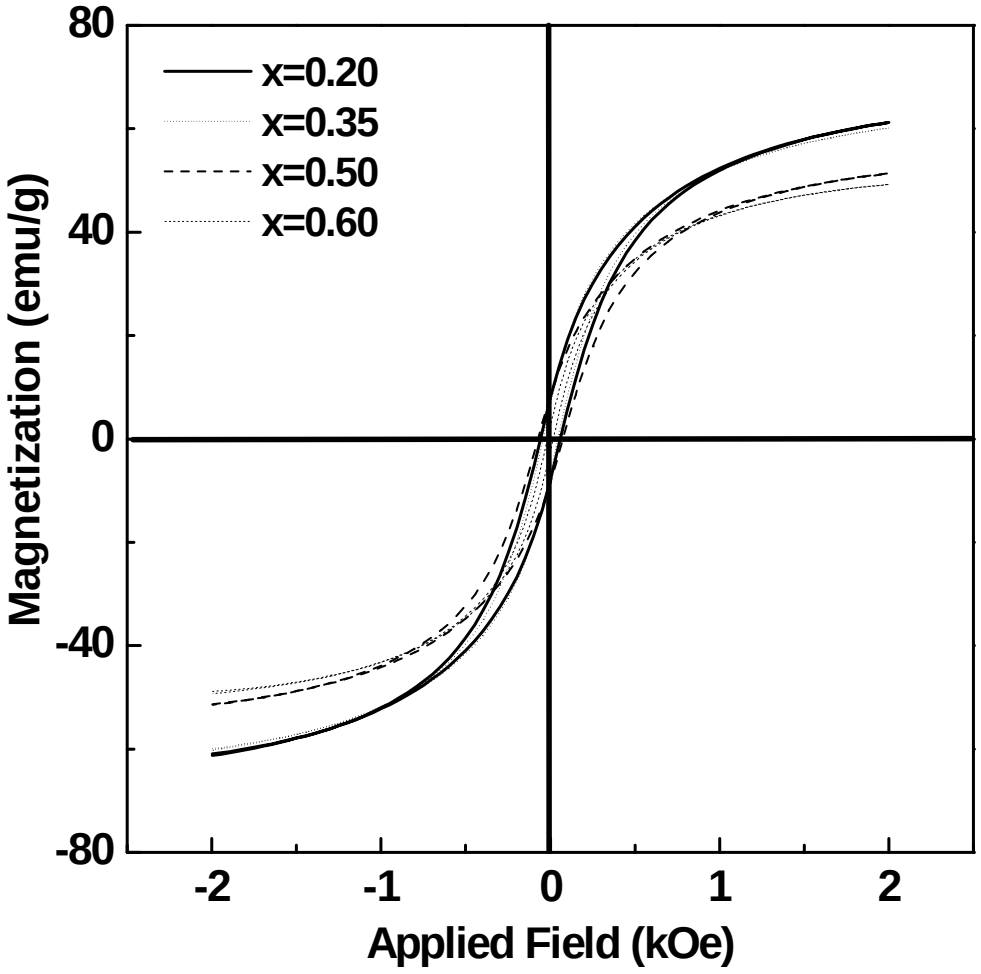

Fig 5.7 Room temperature hysteresis loops for the series of $Ni_{1-x}Zn_xFe_2O_4$ nanopowders.

It was observed that, the saturation magnetization decreased with increasing Zn^{2+} concentration (x= 0.20 - 0.60) from 61.1 to 49.3 emu/g. Zn^{2+} ions have an affinity to occupy tetrahedral (A) sites and Ni^{2+} ions have a tendency to go into the octahedral (B) sites in the crystal lattice, [44] while Fe^{3+} ions are distributed over both the sites. It might happen that as the concentration of diamagnetic Zn^{2+} on A sites is increased, the Fe^{3+} ions were pushed from A to B sites. This decrease in the magnetic ions at A site resulted in a weakened A-B exchange coupling and hence a diminished moment [43, 133].

Discussion:

TG-DTG-DSC, XRD and TEM analyses of the synthesized precursors and calcined powders confirmed that oxidative decomposition of precursor leads to the formation of single-phase Ni-Zn ferrite nanopowders. The chemical process starts from homogeneous distribution of metal ions in solution. Sucrose serves as a chelating agent and ensures that water-soluble metal ions are uniformly anchored in the polymeric network structure of PVA. This possibly serves to prevent their segregation or any intermittent precipitation from the homogeneous precursor solution during evaporation. A fluffy mass forms due to complete evaporation of the solution, which is effectively a carbonaceous material having a porous structure [57, 123, 133].

During decomposition of these metal ion-containing precursors, nascent metal oxides forms, which are small atomic clusters with proper chemical homogeneity, imbedded in this porous carbonaceous material. These nascent metal oxides finally produce desired single-phase Ni-Zn ferrite nanopowders. The decomposition of carbonaceous material produces gases (such as CO, CO_2, NO_X and water vapor) that help the precursor material to dissipate the heat of combustion and thus inhibit the sintering of fine particles during the process to produce nanosized oxides [57, 123, 133].

DC resistivity measurements indicated that it was strongly correlated with the sintering condition and the composition and hence the microstructure of the samples. The resistivity of the nanopowders was found to be affected by moisture due to their high porosity and low green density (~3g/cm^3). However, for the samples sintered at 1100^0C, the effect of moisture was less pronounced as sintering results in densification (sintered density~3.2-4.0 g/cm^3) and grain

growth. For the samples sintered at an even higher temperature of 1200^0C, the effect of moisture was absent (sintered density ~3.8-4.2 g/cm^3) and the samples exhibited the typical NTCR behavior of ferrites.

5.3 Summary of Results:

1. Ni-Zn ferrite nanopowders were successfully synthesized by using polymer precursor based synthesis route.
2. Major thermal decomposition of the precursor was completed at ~550^0C.
3. Single phase Ni-Zn ferrite was formed at a calcination temperature of 950^0C for two and a half hours in air atmosphere.
4. Average particle size of the nanopowders was ~ 50 nm.
5. Surface morphology studies revealed that the nanoparticles were round in shape.
6. Room temperature resistivity of as-synthesized nanopowder was ~10^6 - 10^7 Ω cm.
7. Room temperature saturation magnetization varied in the range of 49.3 to 61.1 emu/g and the coercivity varied between 16.3 and 73.1 Oe depending on the composition.